Soft Magnetic Tactile Skin for Continuous Force and Location Estimation Using Neural Networks

Tess Hellebrekers ⓘ, Nadine Chang, Keene Chin, Michael J. Ford, Oliver Kroemer ⓘ, and Carmel Majidi ⓘ

Abstract—Soft tactile skins can provide an in-depth understanding of contact location and force through a soft and deformable interface. However, widespread implementation of soft robotic sensing skins remains limited due to non-scalable fabrication techniques, lack of customization, and complex integration requirements. In this work, we demonstrate magnetic composites fabricated with two different matrix materials, a silicone elastomer and urethane foam, that can be used as continuous tactile surfaces for single-point contact localization. Building upon previous work, we increased the sensing area from a 15 mm^2 grid to a 40 mm^2 continuous surface. Additionally, new preprocessing methods for the raw magnetic field data, in conjunction with the use of a neural network, enables rapid location and force estimation in free space. We report an average localization of 1 mm^3 for the silicone surface and 2 mm^3 for the urethane foam. Our approach to soft sensing skins addresses the need for tactile soft surfaces that are simple to fabricate and integrate, customizable in shape and material, and usable in both soft and hybrid robotic systems.

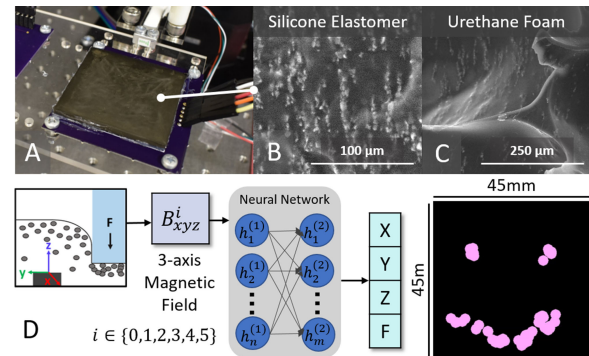*Index Terms*—Soft sensors and actuators, force and tactile sensing, soft robot materials and design.

Fig. 1. (A) Photograph of magnetic elastomer tactile surface with six underlying magnetometers. Micrographs of cross-sections of (B) silicone elastomer and (C) urethane foam embedded with magnetic micro-particles aligned along a magnetic field during curing. (D) The magnetometers detect changes in magnetic field caused by localized contact that can be localized through a neural network and visualized on-screen.

I. INTRODUCTION

TACTILE sensors provide critical information to robotic systems about their environment, which includes nearby objects, obstacles, and people. Soft tactile sensors represent an emerging subclass of tactile sensors that employ deformable and compliant materials at the interaction surface. This added compliance not only passively responds to rich environmental information but also contributes effective mechanical properties shown to enable successful robotic manipulation [1]–[3],

Tess Hellebrekers, Nadine Chang, Keene Chin, and Oliver Kroemer are with the Robotics Institute, School of Computer Science, Carnegie Mellon University, Pittsburgh, PA 15123 USA (e-mail: tessh@andrew.cmu.edu; nchang1@cs.cmu.edu; keenec@andrew.cmu.edu; okroemer@andrew.cmu.edu).

Michael J. Ford is with the Department of Mechanical Engineering, Carnegie Mellon University, Pittsburgh, PA 15213 USA (e-mail: mford2@andrew.cmu.edu).

Carmel Majidi is with the Robotics Institute, School of Computer Science, Carnegie Mellon University, Pittsburgh, PA 15123 USA, and also with the Department of Mechanical Engineering, Carnegie Mellon University, Pittsburgh, PA 15213 USA (e-mail: cmajidi@andrew.cmu.edu).

This article has supplementary downloadable material available at http://ieeexplore.ieee.org, provided by the authors.

Digital Object Identifier 10.1109/LRA.2020.2983707

human-robot interaction [4], [5], and material classification [6], [7], among many others. Soft tactile sensors draw from a variety of transduction modes, most commonly optical [8]–[10], resistive [11], [12], and capacitive [13]. While each approach includes unique advantages and disadvantages, they share a common barrier to scalability. This challenge to scalability can stem from any combination of the following: complex fabrication techniques, weak soft-rigid interfaces, material/fluid leakage, and bulky accessory equipment. For example, optical systems provide very detailed information but require bulky hardware limited by the fixed focal distance of the camera. In the case of arrays of resistive or capacitive sensing skins, the increased density of each unit is linked to an unmanageable scaling in wiring and failure at weak soft-rigid electrical interfaces.

Magnetic sensing is particularly interesting for its ability to support high resolution, high speed sensing, and limited dependency on direct electrical wiring [14]. Recent advancements in commercial magnetometers provide high sensitivity and range in thin (<1 mm) and inexpensive (<2 USD) formats. Unlike discrete taxel arrays, magnetic flux detection is dependent only on proximity of the magnetic field source, which provides a continuous volume of electromagnetically transmitted sensing data and thereby circumvents the need for soft-rigid electrical connections. However, magnetic sensors are generally quite susceptible to environmental noise and only sensitive within a limited volume. Nonetheless, with appropriate filters for ambient magnetic noise, magnetic soft tactile sensors are a promising approach to accurate and responsive tactile skins for robotic
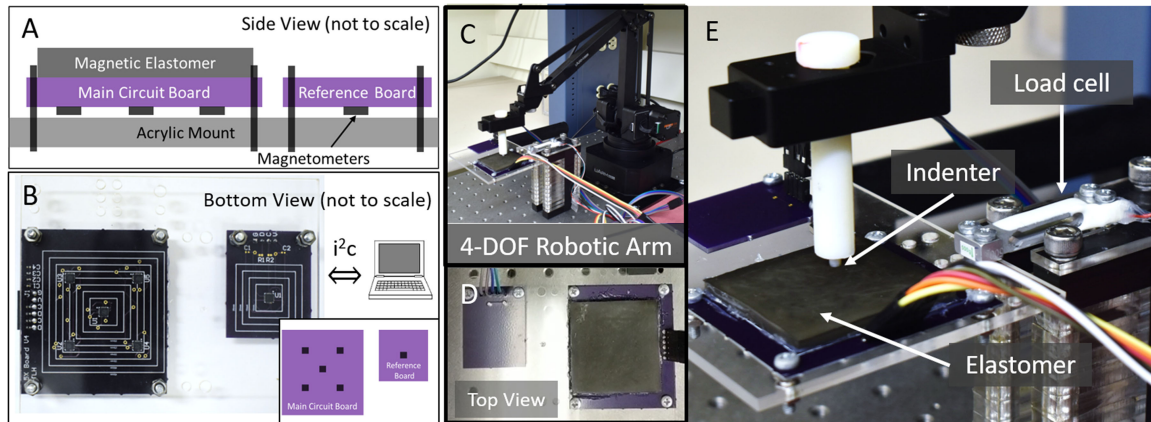
Fig. 2. (A) Schematic cross-section of the magnetometers on the bottom side of the circuit boards and the magnetic elastomer on the top side of the circuit board. (B) Photograph and schematic of bottom view depicting five magnetometers laid out on the main board to sense changes in the magnetic elastomer, along with a single magnetometer used for reference outside the skin's signal range. (C) Photograph of the experimental set-up, which uses 4-DOF robot arm to collect spatial position and (D) top-view photograph of reference board (left) and main board (right). (E) Detailed setup with spherical indenter (D = 3 mm), load cell, and $45 \times 45 \times 3$ mm^3 sensing skin.

sensing applications. For the above reasons, we consider functionalized elastomers with embedded magnetic microparticles. When the magnetic elastomer is deformed, the internal magnetic field is uniquely changed due to the displacement and reorientation of the embedded magnetic microparticles. These changes in magnetic flux can be measured without direct electrical connections and are used to estimate both force and contact location. We show that magnetic elastomers provide a continuous surface for force and contact localization when used in conjunction with digital flux measurement chips.

Previously, we demonstrated a proof-of-concept magnetic elastomer skin for force and location classification and regression [15]. Here, we build significantly upon our previous work by expanding the functional surface area from 15 mm^2 discrete grid to a 40 mm^2 continuous area using multiple magnetometers (Fig. 1A). We demonstrate our approach using two different matrix materials, a silicone elastomer and urethane foam, loaded with magnetic microparticles for a tactile sensing application.Critically, our updated implementation introduces an effective approach to reduce ambient magnetic noise from motion ($\sim$6$\times$) and incorporates neural networks for real-time output and improved localization ($\sim$7.5$\times$ for silicone and $\sim$3$\times$ for foam). The board interface of the current design requires only six output wires to communicate all of the data with the microcontroller. The generalization of this technique allows for a wide range of material choices that lead to user-selectable range and resolution with applied force.

II. RELATED WORK

Magnetic tactile sensors typically measure contact displacement through changes in either magnetic flux or electromagnetic induction [16]. Soft magnetic tactile sensors most commonly combine a Hall-effect sensing chip with a discrete permanent magnet suspended in between two elastomer layers [17], [18]. The position of the permanent magnet is tracked by the 3-axis

magnetic flux to detect applied shear and normal forces [19], [20]. Air gaps between the magnet and sensor enable very low forces (μN scale) to be detected [21].

The work presented here differs from previous work by combining a digital magnetometer with a homogeneous soft skin that contains randomly distributed magnetic microparticles. The microparticles minimize internal stress concentrations and the risk of delamination that can occur around the embedded macroscale magnets. The millions of particles distributed throughout the composite represent input data that are ultimately reduced to a 3-axis magnetic field measurement. By focusing on 3-axis magnetic field measurements, the skin leverages morphological computation and ignores the complex interactions occurring within the skin itself. Notably, the overall magnetic strength of the magnetic elastomer is much less than a permanent magnet. However, due to the current range and resolution of commercially available magnetometers, the signal magnitude remains sufficient to localize contact and estimate force over the surface. Lastly, this technique does not require multi-layer molding and imposes very few limitations on shape, size, or thickness.

While the particles are shear-mixed for a uniform distribution, clusters can still occur in each sample, creating a unique magnetic field (Fig. 1B,C). The magnetic field changes can also differ due to the deformation of different particle clusters (e.g., a +x contact could register differently than a -x contact due to localized clusters). For this reason, magnetic modeling techniques that depend on symmetry of the system are not able to successfully capture the unique signals of each sample. As an alternative, machine learning techniques have become increasingly popular for characterizing the non-linear properties of soft sensors [22], unpredictable deviations between samples [23], and hard-to-interpret tactile signals [24], [25]. Due to the non-linearity of the host elastomers, combined with the unpredictable distribution of magnetic particles, we chose a learning approach to capture the unique pattern of contact signals over each sample's surface (Fig. 1D).
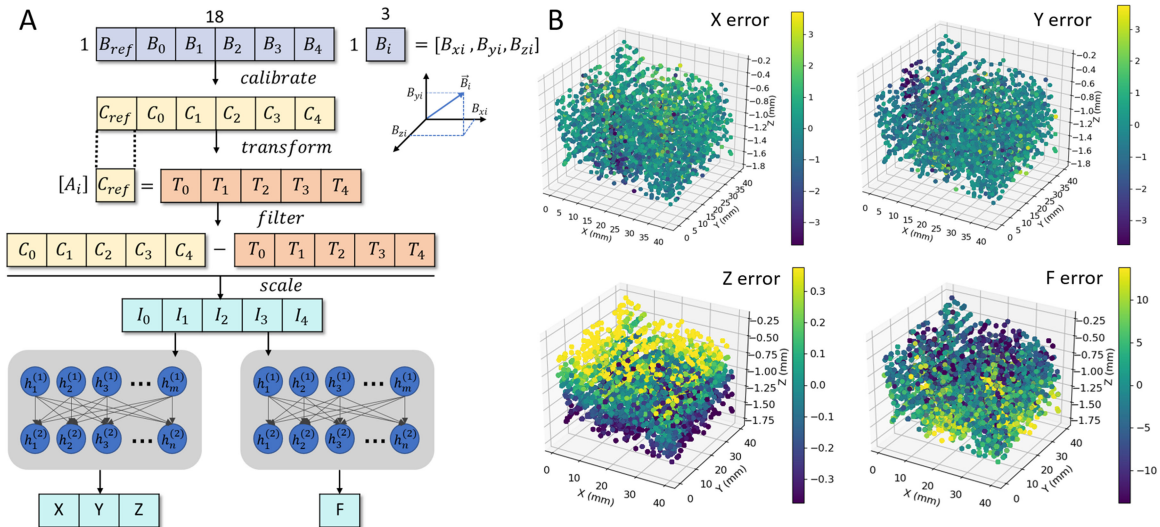
Fig. 3.   (A) A summary of preprocessing steps for contact localization and force estimation. The raw magnetometer values are calibrated individually, transformed from the reference signal, filtered, and scaled for neural network input (See Section IV-A for more details) (B) Estimation error (colormap) plotted against spatial location (axes) for silicone elastomer sample. The units of the colormap are mm for X, Y, and Z errors and grams for F error.

III. EXPERIMENTAL DESIGN AND FABRICATION

At a high-level, the magnetic elastomer is adhered to the backside of a rigid circuit board with five digital magnetometers. A reference magnetometer, with no skin, remains rigidly fixed 4 cm away relative to the main board, and records ambient magnetic noise. The reference signal combined with the main board isolates changes in magnetic flux due to deformation of the magnetic elastomer. These signals are then evaluated by a previously trained neural network to provide real-time estimates of force and location.

A. Circuit Board

The circuit board underneath the magnetic elastomer contains five identical magnetometer chips (MLX90393; Melexis) spaced approximately 15 mm apart (Fig. 2A,B). 15 mm was selected as the maximum range before the signal of the magnetic elastomer can no longer be detected by a central chip [15]. Each 15 mm range overlaps with the neighboring chip's range by 2.5 mm to maximize functional surface area, minimize the required number of chips, and provide redundant signal for relatively weaker edge contacts. This arrangement of chips at the four corners and center also maximizes functional surface area while minimizing the required number of chips for a symmetric implementation. Following the manufacturer's specifications, it is possible to place up to 4 of the same chip on the same I^2C bus. In this implementation, the four corner chips share one bus, and the center chip and reference chip share one bus, both of which are sampled from the same microcontroller (Arduino Zero). Each magnetometer measures its surrounding magnetic field in the x-, y-, and z-directions. Every line of data printed over serial communication includes 3-axis information from each magnetometer, for a total of 18 values. The built-in temperature compensation in the chip eliminates the influence of changes in ambient temperature on the magnetic field.

B. Magnetic Elastomer

Both elastomer samples are functionalized by adding magnetic microparticles before curing. The silicone elastomer (Ecoflex 00-30; Smooth-On) and urethane foam (FlexFoam-iT! X; Smooth-On) are both available in two-part prepolymer and curing agent sets. The magnetic microparticles (MQP-15-7-20065; Magnequench), prepolymer, and curing agents are mixed in a 2:1:1 weight ratio. Both composites are then poured into a 45 × 45 × 3 mm 3D-printed mold (Objet24; Stratasys) and cured on top of a 2 × 2 × 0.5 inch permanent magnet (N52; Applied Magnets) magnetized through the thickness. More details on magnetic elastomer fabrication can be found in [15].

The sensing principle is based on the motion of magnetic micro-particles induced by deformation of the host elastomer caused by external pressure. The deformation can be measured as a change in magnetic flux in three directions. The neural network then relates the current magnetic flux state to the location and force of contact.

C. Robot Arm

In order to find the relationship between location and magnetic field, we need to sample across the full surface with a ground truth location. The uArm Swift Pro is a low-cost 4-DOF desktop robotic arm (Fig. 2C). Due to the small workspace and low applied load, the uArm is sufficiently precise to automate the data collection process of the tactile skin and provide ground truth location. A 3D-printed spherical indentor (D = 3 mm) was placed in the universal gripper clamp. The robot arm position was calibrated using guide points in the acrylic plate (Fig. 2D, E).

D. Data Collection

A 1-axis load cell (TAL221; Sparkfun) supported an acrylic plate with both the magnetic skin board and reference

magnetometer. The load cell is calibrated and tared at the beginning of the data collection. During data collection, the force output confirms that the robot arm has made contact with the skin before recording samples and is used as a ground truth applied force. 3000 locations inside a $40 \times 40 \times 1.5$ mm^3 volume of the sample, starting 0.5 mm below the surface, were randomly selected from a uniform distribution and then rounded to the first decimal point. The robot arm was directed to each location, and 100 samples were recorded at 10 Hz. The magnetometer data, current encoder position of the robot arm, and load cell output were saved to a file. Due to the positional error of the robot arm, the encoder reading position was not exactly the same as the commanded position, but reads within the expected error (<0.5 mm) of the system. In total, data collection took about 24 hours for each of four samples: plain ecoflex, magnetic ecoflex, plain foam, and magnetic foam. The 'plain' refers to silicone elastomer and urethane foam samples made without magnetic microparticles as control groups, and 'magnetic' refers to silicone elastomer and urethane embedded with magnetic microparticles.

IV. SIGNAL PROCESSING

Our approach combines calibration and preprocessing techniques to minimize the amount of data collection necessary while keeping the neural network input limited to raw magnetometer data. First, we calibrate the magnetometers individually using standard techniques and approximations outlined by Hemanth *et al.* [26]. Then, we filter the calibrated signals using a transformed reference signal. Finally, we scale the filtered, calibrated signals for the neural network model. The affine transformation between boards remains valid while the two boards remain fixed relative to one another.

A. Preprocessing

Each magnetometer outputs three axis data, B_i, about its surrounding magnetic field. This implementation includes six individual magnetometer chips, for a total of 18 datapoints per sample.

$$B_i = [B_{xi}, B_{yi}, B_{zi}] \tag{1}$$

for i from 0 to 5. Previously, we collected calibration values from the 'figure 8' motion to determine scaling, s_i, and offset, o_i parameters for each of the magnetometers. First we applied these to the raw data to calibrate the signals individually

$$C_i = [s_{xi}, s_{yi}, s_{zi}] . * [B_i] - [o_{xi}, o_{yi}, o_{zi}] \tag{2}$$

for i from 0 to 5 where C_i is a 3x1 vector for the calibrated data from each magnetometer. Offsets were determined by the average between the maximum and minimum signals in each direction. Scales were determined by dividing the average chord distance in all three directions by the average chord length in each direction. For example,

$$o_{xi} = \frac{(\max_x + \min_x)}{2} \tag{3}$$

$$s_{xi} = \frac{(\max_x - \min_x) + (\max_y - \min_y) + (\max_z - \min_z)}{(\max_x - \min_x)} \tag{4}$$

TABLE I
5-FOLD VALIDATION RESULTS FOR XYZ NEURAL NETWORK

skin type	input data	RMSE (mm)	MAE (mm)
'magnetic ecoflex'	training	3.32±0.10	0.86±0.03
	testing	3.82±0.26	0.96±0.05
'plain ecoflex'	training	41.30±0.10	4.23±0.02
	testing	41.97±0.47	4.26±0.02
'magnetic foam'	training	13.77±0.19	1.98±0.03
	testing	15.14±0.35	2.08±0.03
'plain foam'	training	46.47±0.38	4.52±0.02
	testing	47.08±1.25	4.55±0.06

for i from 0 to 5. Next, we applied the affine transform of the reference magnetometer onto the five magnetometers underneath the magnetic skin.

$$A^i \begin{bmatrix} B_x^{ref} \\ B_y^{ref} \\ B_z^{ref} \\ 1 \end{bmatrix} = \begin{bmatrix} B_x^i \\ B_y^i \\ B_z^i \\ 1 \end{bmatrix} \tag{5}$$

for i from 1 to 5. As long as the reference magnetometer stays fixed relative to the magnetic skin circuit board, this transformation allows motion and ambient noise removal due to location and environmental noise. These 15 values represent magnetic noise due to motion and environment and were subtracted from the calibrated values C_i for i 1 to 5. Additionally, this noise removal allows the data collection to occur in one plane.

With the data calibrated and filtered, we prepared the data for neural net input by removing the mean and scaling to unit variance determined from the training data (Fig. 3A).

B. Neural Network

Initially, the techniques outlined in [15] were promising but did not handle the additional non-linearities present in this multi-magnetometer system (Table I, Linear Regression). We attribute the increased non-linearity to the increased size of the data inputs and more complex interactions between the chips and skin. In general, neural networks have been shown to successfully classify and estimate tactile data in a number of examples [27], [28]. For our task, we are specifically interested in estimating location and force at a single-point in time. To that end, we selected a multi-layer perceptron implemented in sklearn with MLPRegressor. Convolutional and recurrent neural networks were not considered due to the small input feature size and quasi-static data collection method.

A shallow sweep across first layer size (over 20, 50, 100, 150, and 200 units), second layer size (over 20, 50, 100, 150, 200 units), activation function (over tanh, relu, logistic), and batch size (over 20, 50, 100, 150, and 200) was evaluated with 5-fold validation to determine the best performing network. Ultimately, a structure of 150 and 200 units for the first and second hidden layers respectively, tanh activation functions, and batch sizes of 20 were selected for good performance across both sample training and testing sets. Two neural networks were trained
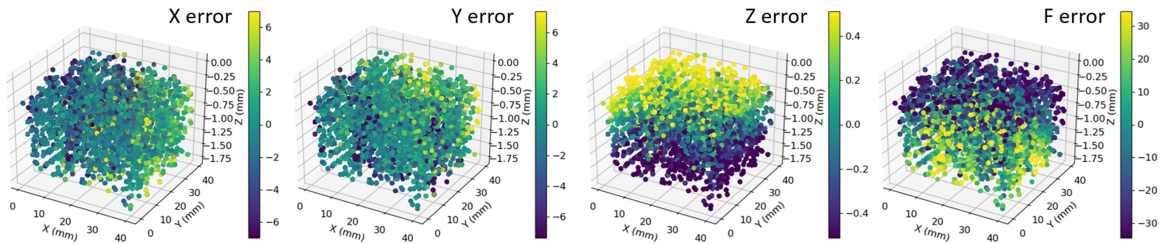
Fig. 4. Estimation error (colormap) plotted against spatial location (axes) for urethane foam sample. The units of the colormap are mm for X, Y, and Z error and grams for F error.

TABLE II
XYZ AND F NEURAL NETWORKS MEAN ABSOLUTE ERRORS AND STANDARD DEVIATION

skin type	model	input data	XYZ (mm)	X (mm)	Y (mm)	Z (mm)	F (g)
'magnetic ecoflex'	linear regression	training (75%)	6.44±6.17	9.58±5.50	9.23±5.57	0.51±0.34	12.21±8.95
		testing (25%)	6.45±6.16	9.56±5.49	9.27±5.55	0.51±0.34	12.27±9.09
'magnetic foam'	linear regresion	training (75%)	5.77±6.07	8.82±5.87	7.99±5.84	0.52± 0.37	27.87±19.59
		testing (25%)	5.79±6.07	8.84±5.86	7.98± 5.85	0.52±0.37	27.85±19.66
'magnetic ecoflex'	neural network	training (75%)	0.85±1.60	1.15±1.91	1.16±1.87	0.25±0.17	6.62±6.53
		testing (25%)	0.86±1.62	1.15±1.88	1.19±1.94	0.25±0.17	6.73±6.72
'magnetic foam'	neural network	training (75%)	1.98±3.12	2.69±3.47	2.83±3.78	0.40±0.30	22.55±17.22
		testing (25%)	2.02±3.23	2.76±3.62	2.89±3.78	0.41±0.30	22.94±17.55

each of the four samples. One estimates the XYZ position in millimeters, and the other estimates the force in grams.

V. RESULTS AND DISCUSSION

As shown in Table I, it is clear that the signal for localization and force is attributed to the addition of magnetic microparticles, and not unintended noise from our experimental setup. Both the 'plain ecoflex' and 'plain foam' samples show much larger error and variance consistently across the 5-fold validation. Both the 'magnetic ecoflex' and 'magnetic foam' samples are able to localize the single-point contact to a 1 mm^3 and 2 mm^3 volume, respectively. Across the 5-fold validation, the root mean-squared error (RMSE) and mean absolute error (MAE) are consistent, showing that the results are not sensitive to the training/testing splits. The results of the magnetic samples split into the individual components of X, Y, Z, and F are shown in Table II. Results between training and testing data sets show minimal overfitting, which may be further improved by increasing the dataset and widening the neural network sweep.

For the silicone elastomer soft skin, we report a mean absolute X error of 1.15 ± 1.91 mm, Y error of 1.16 ± 1.87 mm, and Z error of 0.25 ± 0.17 mm (Table II Magnetic Ecoflex). The error variance is relatively large compared to the mean but is small relative to the skin area and still represents good localization of the contact area (Supplementary Video). The Z error is lower due to the cubic relationship between strength of magnetic signal with distance and the higher z-axis sensitivity of the magnetometers. For the urethane foam soft skin, we report a mean absolute X error of 2.69 ± 3.47 mm, Y error of 2.83 ± 3.78, and Z error of 0.40 ± 030 (Table II Magnetic Foam). The mean and variance of the error for the urethane foam is larger across all outputs compared to the silicone sample. We
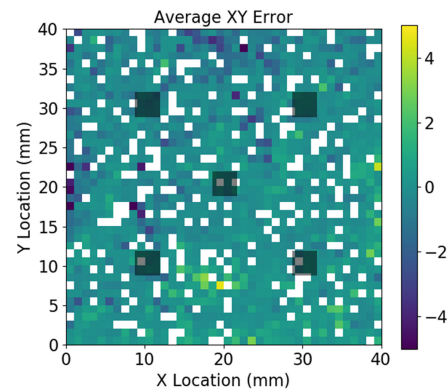

Fig. 5. Average XY error displayed for 40x40 mm silicone sample in 1 mm^2 bins. Regions of highest error are generally on the edge of the skin and edges between magnetometers, locations overlaid in transparent boxes.

attribute this difference to the urethane foam curing process. During curing, the foam introduces bubbles into the sample that will displace the magnetic particles. The stochastic nature of this process creates a sample with less uniformity, and therefore more complicated relationship between deformation and magnetic field. Still, the testing set results show that the magnetic foam sample can localize to within a 2 mm^3 volume on average, which is a reasonable trade-off for a more robust surface the urethane foam provides over the silicone.

True error (negative and positive) for the X, Y, Z, and F (force) estimates are displayed spatially in 3D space for the silicone elastomer (Fig. 3B) and urethane foam (Fig. 4). Each colormap for the error spans two standard deviations from the data, and therefore represents 95% of the data. Across the X and Y surfaces, we see similarly low errors for locations immediately surrounding the five magnetometers. When contact is closer to

TABLE III
XYZ NEURAL NETWORKS MAE ACROSS INDENTER DIAMETER

		Testing MAE (mm)	
		D=3	D=6
Training	D=3	0.79±1.00	1.52±1.86
MAE (mm)	D=6	2.70±4.49	0.56±0.52

the chips, the signal will be larger and easier to estimate. At the edges farthest away from the chips, there are two oddly large areas of error, shown in dark blue at the top center and left center edges (Fig. 5).This larger error can be attributed to a combination of distance from the chip and uneven magnetic particle distribution degrading the signal. Lastly, we collected an additional dataset with indenter size (D = 6 mm) to compare results across indenter size. Results show that the larger indenter can achieve higher spatial accuracy due to the larger contact deformation. However, the larger indenter has a much lower accuracy when generalizing to unseen data from the smaller indenter (Table III).

One key advantage of the skin relative to other tactile skins is that the magnetic field sensing does not require direct electrical contact. However, this advantage is directly coupled with susceptibility to nearby magnetic noise. Magnetized objects cause undesired aliasing, whereas metals (e.g. aluminum and stainless steel) introduce only minimal noise that do not significantly affect the model's performance (Supplementary Video). Similarly, the skin requires a reference signal to filter static ambient fields. However, not all robotic systems will accommodate a reference board nearby the magnetic elastomer, nor can it be assumed that both boards are being exposed to the same ambient noise. In this case, the known robot orientation can also be used to remove the ambient noise from motion. Finally, the magnetic flux changes are coupled to the deformation of the host elastomer. Therefore, time- and rate-dependent properties of the elastomer that arise from viscoelasticity, such as creep and relaxation, may result in drift or hysteresis of the sensing skin. Overall consistency and robustness of the magnetic signal will be dependent on the choice of host elastomer.

VI. DEMONSTRATIONS

A. Motion Filter

For practical implementation of the soft magnetic skin, the skin should operate consistently when subjected to motion in 3D space. However, the neural network cannot differentiate between changes in magnetic flux due to motion and skin deformation. A motion filter represents a simple way to remove ambient magnetic noise before utilizing the neural network, simplifying data collection and practical use of the tactile sensor. In Fig. 6A, we show a significant reduction of noise, from approximately ±30 to ±5 μT, when the urethane foam sample is rapidly moved in 3D space without deforming the skin's surface. The noise after filtering the motion is comparable to the inherent noise of the chip, and the neural network generalizes this well, as shown in the Supplementary Video.
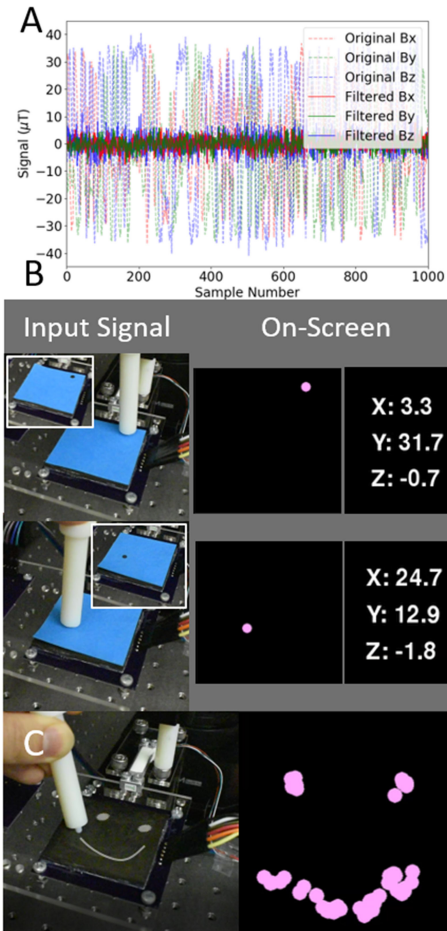

Fig. 6. (A) Magnetic signal for each sample with (solid lines) and without (dashed lines) the motion filter. (B) Photographs of stencil pressing where the input signal is shown along with the corresponding on-screen pattern detected by the soft skin. (C) Photographs from drawing a smiling face shown along with the corresponding pattern detected by the soft skin.

B. Single-Point Contact

To highlight the ability of the skin to detect contact, we tested by manually applying single-point contacts. In Fig. 6, we have loaded the neural network trained on previous data from the robotic arm. The magnetometers are being sampled at 25 Hz and passed to a computer via serial communication. The data is preprocessed and then the XYZ and F are estimated. The localization works well in practice, consistent with the X,Y,Z, and F error plots discussed previously. In Fig. 6B, we display the one pink dot to represent most recent XYZ estimation to the screen corresponding to the overlaid paper stencil. In Fig. 6C, we display a history of all previous XYZ estimations corresponding to a hand-drawn smiley face. The Supplementary Video includes both of these demonstrations to convey a more dynamic understanding of the jitter and drift for both the silicone and urethane foam sensing skins.

C. Writing Numbers

Finally, the skin should be capable of dynamic measurements as well as the static inputs considered thus far. We demonstrate a simple task of classifying digits through writing on soft skin,

which illustrates the ability of identifying meaningful change through temporal space. We train an support vector machine (SVM) to classify raw magnetometer data directly into written numbers 0–9, without the previously discussed XYZ neural network. The trained SVM has a final accuracy of 92.86% on our held-out test set. In our demonstration, we further showcase the SVM success in a real-time setting. A short real-time demonstration is included in the Supplementary Video. All collected data and collecting, preprocessing, and SVM code are publicly available on github (https://github.com/nchang430/magnetic_skin).

VII. Conclusions and Future Work

In conclusion, we have shown an effective technique for fabricating and interpreting data from a magnetic tactile skin for single-point contact localization and force estimation. Key improvements from previous work include scaling up the design with minimal interface changes, a simple calibration and filter routine to enable motion in free space, and a learning strategy that can successfully handle the multi-chip system. The system can be customized for different applications by adjusting the shape and size of the skin or tiling up multiple smaller modules. The data-driven methods can also be adapted to train implementations to react to any desired deformations, given a reference ground truth signal.

In the future, we plan to expand the work to include multi-point contacts. For our system, a multi-contact signal is equivalent to the vector addition of all the single-contact signals. Techniques for vector decomposition in conjunction with the finite signal space will be explored to identify the individual contact components. We are also interested in improving the experimental setup to provide ground truth for 6-DOF force and torque measurements. The ability to discern both normal and shear forces is valuable in moving towards a low-cost tactile module for robotic manipulation and particularly useful for the unconstrained motion of soft robotics. Lastly, the integration of the magnetic skin with existing stretchable circuitry [29] will lead to sensing capabilities previously not available in a soft format.

Acknowledgment

References

[1] W. Chen, H. Khamis, I. Birznieks, N. F. Lepora, and S. J. Redmond, "Tactile sensors for friction estimation and incipient slip detection-toward dexterous robotic manipulation: A review," *IEEE Sensors J.*, vol. 18, no. 22, pp. 9049–9064, Nov. 2018.

[2] E. Torres-Jara and L. Natale, "Sensitive manipulation: Manipulation through tactile feedback," *Int. J. Humanoid Robot.*, vol. 15, no. 01, 2018, Art. no. 1850012.

[3] Z. Su, K. Hausman, Y. Chebotar, A. Molchanov, G. E. Loeb, G. S. Sukhatme, and S. Schaal, "Force estimation and slip detection/classification for grip control using a biomimetic tactile sensor," in *Proc. IEEE-RAS 15th Int. Conf. Humanoid Robots*, 2015, pp. 297–303.

[4] K.-U. Kyung and S.-Y. Kim, "Soft sensors and actuators for designing new human-robot/machine interaction interfaces," in *Proc. 14th ACM/IEEE Int. Conf. Human-Robot Interaction*, 2019, pp. 695–695.

[5] T. Arnold and M. Scheutz, "The tactile ethics of soft robotics: Designing wisely for human–robot interaction," *Soft Robot.*, vol. 4, no. 2, pp. 81–87, 2017.

[6] D. S. Chathuranga, Z. Wang, Y. Noh, T. Nanayakkara, and S. Hirai, "Robust real time material classification algorithm using soft three axis tactile sensor: Evaluation of the algorithm," in *Proc. IEEE/RSJ Int. Conf. Intell. Robots Syst.*, 2015, pp. 2093–2098.

[7] E. Kerr, T. M. McGinnity, and S. Coleman, "Material recognition using tactile sensing," *Expert Syst. Appl.*, vol. 94, pp. 94–111, 2018.

[8] B. Ward-Cherrier *et al.*, "The tactip family: Soft optical tactile sensors with 3d-printed biomimetic morphologies," *Soft Robot.*, vol. 5, no. 2, pp. 216–227, 2018.

[9] C. To, T. L. Hellebrekers, and Y.-L. Park, "Highly stretchable optical sensors for pressure, strain, and curvature measurement," in *Proc. IEEE/RSJ Int. Conf. Intell. Robots Syst.*, 2015, pp. 5898–5903.

[10] W. Yuan, S. Dong, and E. Adelson, "Gelsight: High-resolution robot tactile sensors for estimating geometry and force," *Sensors*, vol. 17, no. 12, 2017, Art. no. 2762.

[11] B. Shih, J. Mayeda, Z. Huo, C. Christianson, and M. T. Tolley, "3d printed resistive soft sensors," in *Proc. IEEE Int. Conf. Soft Robot.*, 2018, pp. 152–157.

[12] M. D. Dickey, "Stretchable and soft electronics using liquid metals," *Adv. Mater.*, vol. 29, no. 27, 2017, Art. no. 1606425.

[13] A. Frutiger *et al.*, "Capacitive soft strain sensors via multicore–shell fiber printing," *Adv. Mater.*, vol. 27, no. 15, pp. 2440–2446, 2015.

[14] J. Lenz and S. Edelstein, "Magnetic sensors and their applications," *IEEE Sensors J.*, vol. 6, no. 3, pp. 631–649, Jun. 2006.

[15] T. Hellebrekers, O. Kroemer, and C. Majidi, "Soft magnetic skin for continuous deformation sensing," *Adv. Intell. Syst.*, vol. 1, no. 4, 2019, Art. no. 1900025.

[16] C. Chi, X. Sun, N. Xue, T. Li, and C. Liu, "Recent progress in technologies for tactile sensors," *Sensors*, vol. 18, no. 4, 2018, Art. no. 948.

[17] C. Ledermann, S. Wirges, D. Oertel, M. Mende, and H. Woern, "Tactile sensor on a magnetic basis using novel 3d hall sensor-first prototypes and results," in *Proc. IEEE 17th Int. Conf. Intell. Eng. Syst.*, 2013, pp. 55–60.

[18] L. Jamone, L. Natale, G. Metta, and G. Sandini, "Highly sensitive soft tactile sensors for an anthropomorphic robotic hand," *IEEE Sensors J.*, vol. 15, no. 8, pp. 4226–4233, Aug. 2015.

[19] T. Paulino *et al.*, "Low-cost 3-axis soft tactile sensors for the human-friendly robot vizzy," in *Proc. IEEE Int. Conf. Robot. Autom.*, 2017, pp. 966–971.

[20] T. Tomo *et al.*, "Design and characterization of a three-axis hall effect-based soft skin sensor," *Sensors*, vol. 16, no. 4, 2016, Art. no. 491.

[21] Y. Wu *et al.*, "A skin-inspired tactile sensor for smart prosthetics," *Sci. Robot.*, vol. 3, no. 22, 2018, Paper eaat0429.

[22] S. Han, T. Kim, D. Kim, Y.-L. Park, and S. Jo, "Use of deep learning for characterization of microfluidic soft sensors," *IEEE Robot. Autom. Lett.*, vol. 3, no. 2, pp. 873–880, Apr. 2018.

[23] S. S. Baishya and B. Bäuml, "Robust material classification with a tactile skin using deep learning," in *Proc. IEEE Int. Conf. Intell. Robots Syst.*, 2016, vol. 2016, pp. 8–15.

[24] B. S. Homberg, R. K. Katzschmann, M. R. Dogar, and D. Rus, "Haptic identification of objects using a modular soft robotic gripper," in *Proc. IEEE/RSJ Int. Conf. Intell. Robots Syst.*, 2015, pp. 1698–1705.

[25] C. Choi, W. Schwarting, J. DelPreto, and D. Rus, "Learning object grasping for soft robot hands," *IEEE Robot. Autom. Lett.*, vol. 3, no. 3, pp. 2370–2377, Jul. 2018.

[26] K. Hemanth, V. Talasila, and S. Rao, "Calibration of 3-axis magnetometers," *IFAC Proc. Volumes*, vol. 45, no. 1, pp. 175–178, 2012.

[27] M. Acer and A. F. Yıldız, "Force localization estimation using a designed soft tactile sensor," in *International Symposium on Wearable Robotics*, Berlin, Germany: Springer, 2018, pp. 8–12.

[28] A. Molchanov, O. Kroemer, Z. Su, and G. S. Sukhatme, "Contact localization on grasped objects using tactile sensing," in *Proc. IEEE/RSJ Int. Conf. Intell. Robots Syst.*, 2016, pp. 216–222.

[29] N. Lu and D.-H. Kim, "Flexible and stretchable electronics paving the way for soft robotics," *Soft Robot.*, vol. 1, no. 1, pp. 53–62, 2014.